Mechanical characterization of drawn Zeonex, Topas, polycarbonate and PMMA microstructured polymer optical fibres

Rasmussen, H. K.; Fasano, A.; Stajanca, P.; Woyessa, G.; Schukar, M.; Bang, O.

Published in:
Optical Materials Express

Link to article, DOI:
10.1364/OME.8.003600

Publication date:
2018

Document Version
Publisher's PDF, also known as Version of record

Research Article | Vol. 8, No. 11 | 1 Nov 2018 | OPTICAL MATERIALS EXPRESS 3600
Optical Materials EXPRESS

Mechanical characterization of drawn Zeonex, Topas, polycarbonate and PMMA microstructured polymer optical fibres

H. K. RASMUSSEN,[1,*] A. FASANO,[1] P. STAJANCA,[2] G. WOYESSA,[3] M. SCHUKAR,[2] AND O. BANG[3,4]

[1]*DTU Mekanik, Department of Mechanical Engineering, Technical University of Denmark, 2800 Kgs. Lyngby, Denmark*
[2]*BAM Bundesanstalt für Materialforschung und -prüfung, Unter den Eichen 87, 12205 Berlin, Germany*
[3]*DTU Fotonik, Department of Photonics Engineering, Technical University of Denmark, 2800 Kgs. Lyngby, Denmark*
[4]*SHUTE Sensing Solutions ApS, Diplomvej 381, DK-2800 Kgs. Lyngby, Denmark*
[*]*hkra@mek.dtu.dk*

Abstract: The mechanical stress-strain behaviour of polymer optical fibres (POFs) drawn from various materials was measured, both before and after temperature annealing of the POFs. The POFs were drawn from PMMA (GEHR), Zeonex (480R), PC (Makrolon LED2245) and two different grades of Topas (8007S-04 and 5013S-04). With fibre drawing stresses at or above the elastic (uniaxial extensional) plateau modulus, the polymer chains in the POFs have a high degree of alignment, which has a large impact on fibre mechanical behaviour. The testing was performed at straining rates ranging from 0.011%/s, to 1.1%/s for the un-annealed fibres and a straining rate of 1.1%/s for the annealed ones. The elastic modulus of the tested POFs showed no sensitivity toward variation of straining rate. In the case of Topas 5013S-04 and PMMA, the producer-reported values are the same as the one obtained here for the POFs both before and after annealing. The drawn POFs made of Zeonex, PC, and Topas 8007S-04 exhibit larger elastic modulus than the respective materials in the bulk form. The elastic modulus of these fibres is reduced upon annealing by 10-15%, but still remains above the producer-reported values for the bulk polymers. In the nonlinear elastic region, only the PC POF is statistically unaffected by the changes in the straining rate, while Topas 8007S-04 POF shows insensitivity to the straining rate until 3% strain. All other changes affect the stress-strain curves. The annealing flattens all stress-strain curves, making the fibres more sensitive to yield.

1. Introduction

In sensor technology Polymer Optical Fibres (POFs) differ from silica-based ones, due to the fundamental differences in chemical and physical properties [1]. POFs have often larger flexibility in bending and straining due to non-brittle nature of polymer materials [2]. They allow diffusion of small molecules in the material, where additive or chemical functionalization can change them into chemical and biochemical detectors [3]. They are also attractive for in-vivo applications as many polymers are biocompatible [4–7] and biodegradable [8]. Particularly microstructured POFs (mPOFs) are highly attractive due to flexibility of their design and relatively straightforward fabrication of single mode fibres [9–11]. Polymethyl methacrylate (PMMA) was the first polymer used for mPOF fabrication [9,2,3], and still remains the most widely used one [12–15]. In recent years, mPOFs from different polymers have been developed having similar low-loss properties as PMMA in the visible and near infra-red spectrum. Examples include Topas (cyclic olefin copolymer) [5,16,17], Polycarbonate (PC) [18] and Zeonex (polynorbornene) [19]. Though, none of these polymers has as low loss as some amorphous fluoropolymers like CYTOP [20,21]. Other

#334388 https://doi.org/10.1364/OME.8.003600
Journal © 2018 Received 4 Jun 2018; revised 2 Oct 2018; accepted 9 Oct 2018; published 30 Oct 2018

Optical Materials EXPRESS

polymers have been used in POFs or mPOFs, and more are likely to be developed in the future.

The low elastic modulus of polymers, compared to glass, increases fibre sensitivity toward stress, which is particularly important in vibration and sound sensing [22,23]. Mechanical strain sensing has been demonstrated with PMMA [12,13,24], Topas [25,16], Zeonex [19], and Polycarbonate [18] mPOFs, based on fibre Bragg grating (FBG) sensing. The mechanical behaviour, the elastic modulus and other nonlinear parameters, of POFs differs from glass-based fibres due to polymers' visco-elastic nature and anisotropy of stretched and oriented polymer chains. The importance of polymer chain orientation for fibre mechanical behaviour has been clearly demonstrated for PMMA POFs [26–28]. Nevertheless, mechanical characteristics of POFs might be considerably material dependent. Therefore, the purpose of this paper is to look at the mechanical stress-strain behaviour of POFs drawn from various materials in order to provide more comprehensive information on POF mechanical performance. In addition to common PMMA POFs, we will study fibres drawn from Topas, Zeonex, and PC that have been demonstrated to be useful in sensing applications [16,19,18,25]. The fibres from different materials having nominally similar (geometrical) characteristics will be tested, both before and after temperature annealing. The attractiveness of Zeonex and Topas fibres lies in their insensitivity to changes in relative humidity, which is a common issue with PMMA POFs [16,19,18]. PC POFs have been developed as an alternative to PMMA POFs due to their higher thermal stability [18]. This study provides new important information for optimal POF selection for applications where consideration of fibre mechanical performance is crucial, e.g. in strain and stress sensing applications. Mechanical characterization of POFs has been done uniquely by extension of the fibres. Classically, as done here, by applying a constant extension rate, though more advanced regimes as dynamic mechanical characterization has been applied recently [29–31].

Table 1. Drawing temperature and stress, fibre diameter (before and after annealing), and annealing temperature.

Fibre material	Drawing temperature	Average drawing stress	Average unannealed fibre diameter	Annealing temperature	Average annealed fibre diameter
PMMA (GEHR)	~178°C	9.8 MPa	152 µm	80°C	155 µm
PC LED2245	~185°C	11.4 MPa	150 µm	125°C	155 µm
Zeonex 480R	~180°C	10.5 MPa	148 µm	120°C	152 µm
Topas 8007S-04	~160°C	9.2 MPa	147 µm	60°C	146 µm
Topas 5013S-04	~175°C	12 MPa	183 µm	115°C	183 µm

2. Polymers and fibre manufacturing

The polymers used in this work for mPOF fabrication are: PMMA (GEHR) [32], Zeonex (480R) [19], PC (Makrolon LED2245) [18] and two different grades of Topas [25,33,16]. PMMA, Zeonex and PC are all homopolymers, whereas Topas is a norbornene-ethylene copolymer. In copolymers, a change in relative composition modifies the properties of the polymer. Here we have used Topas 8007S-04 [34] and Topas 5013S-04 [35] which have glass transition temperature of 78°C and 134°C, respectively. The Zeonex 480R [36] has a glass transition of 138°C and the PC Makrolon LED2245 [37] has a glass transition of 145°C. It is important to refer to the correct trade name and number of the particular polymer, as a change in polymer molecular weight and its distribution will have an effect on the mechanical properties of the polymer.

The fibres were all fabricated in-house by the following consecutive steps: (1) Casting of granular polymers into bulk cylinders, (2) machining the preform into a cylinder of 60 mm in diameter and height of 100 mm, (3) annealing of the preform for 10 days (4) drawing the annealed preform into 6 millimetre in diameter canes, (5) sleeving the cane by a tube made, of about 15 mm in diameter, of the same the preform material and annealed the secondary preform for 7 days (6) and then drawing the secondary preform into fibres. All polymers were cast in house except for PMMA (GEHR), which was bought commercially in the form of a

Optical Materials EXPRESS

rod. The overall aim of the fibre production is to obtain fibres with defined thickness and avoid fluctuation in the diameter along the fibre length. A reasonable production rate is, of course, also a consideration. In this work, we targeted fabrication of POFs with nominally similar geometrical parameters prepared under similar drawing conditions (drawing stress) so the systematic comparison of POFs' mechanical properties can be performed. The main drawing, geometrical and annealing parameters are listed in Table 1 for POFs prepared from the different polymers.

The mPOFs produced here were all based on an initial preform of a diameter of 60 mm, where a solid core was surrounded by tree rings of drilled holes of 3 mm in diameter. These were arranged in a hexagonal lattice with an inter-hole pitch of 6 mm, giving a core size of 9 mm. The final size of the structure depends somewhat on the final diameter of the drawn fibre, but can be calculated for all the individual fibres by scaling the original preform geometrical dimensions by a reduction factor D_i/(60mm·15mm/6mm). D_i is the final (local) diameter of the fibre which is within the range of 130 μm to 200 μm.

2.1 Fibre drawing and polymer alignment

The drawing force and final fibre diameter are well defined parameters that are measured and controlled during drawing, whereas the drawing temperature is a machine setting. The polymers experience a range of different temperatures during the drawing process. Moreover, in the neck-down region, there are large differences in the temperatures and an inhomogeneous temperature and flow field as well [38,39]. The polymers used in this work are all amorphous and their polymer chains will rearrange their configuration during the drawing process. The produced fibre will contain polymer chains in a frozen non-equilibrium state originating from the drawing process. The drawing stress is an average measure of these internal molecular configurations. The measured stress originates from the polymer configurations in the fibre just before the solidification. The amount of polymer alignment in the final fibre in the drawing direction is directly related to the fibre drawing stress. The drawing stresses used in this study are all at the level of 10 MPa, while the uniaxial extensional plateau modulus of the materials (i.e. three times the plateau modulus, G_N^0) is in the range of 1 MPa (PMMA) to 10 MPa (PC) [40]. This indicates a large degree of alignment in the prepared POFs, as the extensional stresses represent values observed in the rubbery zone [41].

Commonly in a production process, the inhomogeneity in the flow and temperature fields will result in an inhomogeneity in the local polymeric configurations and therefore stresses. In the drawing of the fibre from a polymer rod (preform), the flow is affected by the inhomogeneous flow and temperature in the initial part of the neck-down region [42]. The drawing of a fibre from a 15 mm rod down to a fibre of about 0.14-0.19 mm in diameter represents a relative extension, i.e. an engineering strain, of about $\varepsilon = (L - L_0)/L_0 = 10^4$. Here, L is the current length of the fibre and L_0 is the corresponding initial length in the direction of the drawing. In terms of Hencky strain units $\varepsilon_H = \ln(L/L_0)$, values in between 8.7 and 9.3 are obtained. The Hencky strain is on a logarithmic scale and is the classical scale used in extensional flow of polymer melts [43]. One unit on a Hencky scale corresponds to a relative change of the length of e^1 and diameter of $e^{1/2}$. The molecular alignment will be frozen in in the fibre after the first drawing step (preform into cane) and will continue to develop in the second step (cane into fibre). In linear commercial polymers, steady extensional stress originating from the underlying polymeric alignment during an (uniaxial) extension is commonly obtained before a Hencky strain of 5 [43]. In our case, the Hencky strain during the fibre drawing is way above the values giving steady extensional stress. Further a Hencky strain of 5 is considerably less than the extension experienced by the fibre in the second drawing step. A Hencky strain of 5 represent a relative diameter change of

Optical Materials EXPRESS

$(e^{1/2})^5$ or of about 12. With final fiber diameters in the range of 0.14-0.19 mm the Hencky strain of 5 represents the drawing from a diameter of about 2 mm. From this thickness, temperature differences perpendicular to the drawing direction can be assumed negligible and the flow is nearly homogeneous uniaxial extension. Therefore, just before the solidification, the final configurations and resulting stresses in the fibre can be assumed to be homogeneously distributed and only affected by uniaxial extension. Furthermore, the polymer is extended to a level where the changes in its configuration are effectively limited by a maximal extensibility [44], for the part of the polymer which has not reconfigured due to thermal motion in the polymeric chain. Polymers are a dynamic and the reconfigurations originate, in a complex manner, from the local temperatures and extension rates during the drawing process. Notice that time and temperature in polymers are physically linked through the time-temperature superposition principle, so any local extension rate should be referred to a corresponding isothermal drawing at a reference temperature.

2.2 Fibre annealing

An alignment of the polymer chains in the final fibre reduces stability of the fibre dimensions on a long timescale, especially at evaluated temperatures. Therefore, it is common to increase fibre stability by a deliberate thermal [27,42,4,45,46] or solvent-induced annealing [47,48] of the fibre prior to the use. The fibre may retract in length during the annealing and increase in diameter. This is also technically important in the tuning of the wavelength of a Bragg grating in the fibre. Here, all the fibres were annealed thermally for 2 days at material-specific temperatures listed in Table 1. These are conditions similar to the ones used in previous studies [16,19,18,25]. Mechanical testing was performed both on the un-annealed and annealed fibres.

The annealing occurs in a solid state. This effectively rules out the ability of configurational change of the polymers, which is the flow mechanism in the liquid state. The effects of the annealing on elasticity have to happen on a local scale, i.e. on a length scale much smaller than the size of the polymer chains.

3. Tensile testing

The produced fibres were cleaved [49] into a suitable length and mechanically tested by straining them using an in-house built tensile testing machine. The testing machine had one static fibre holder with a load cell for measuring the force and one stepper-motor-driven traveling crosshead with a linear displacement sensor for straining of the fibre. The initial length of the samples was L_0 = 304.5 mm. Due to the very large ratio between the length and diameter of the fibres, the effect of the non-ideal extension near the fixtures can be assumed to be negligible. All measurements here were performed in a monitored open environment, within a temperature range of 23.4°C to 25.6°C (24.5°C ± 1.1°C) and a relative humidity range of 48% to 55%. The produced fibres are not as ideally shaped as is the case for a standard testing sample. Particularly, the fibre diameter fluctuates along the fibre length. The maximal diameter difference along a fibre length of 304.5 mm is commonly about 10%, i.e. ± 5%. The actual fibre thickness was measured at six (N = 6) places equally distributed along the length of the sample. All tested fibres had final local diameters D_i within the range of 130 µm to 200 µm and corresponding local cross-sectional areas of $A_i = \pi D_i^2 / 4$.

Optical Materials EXPRESS

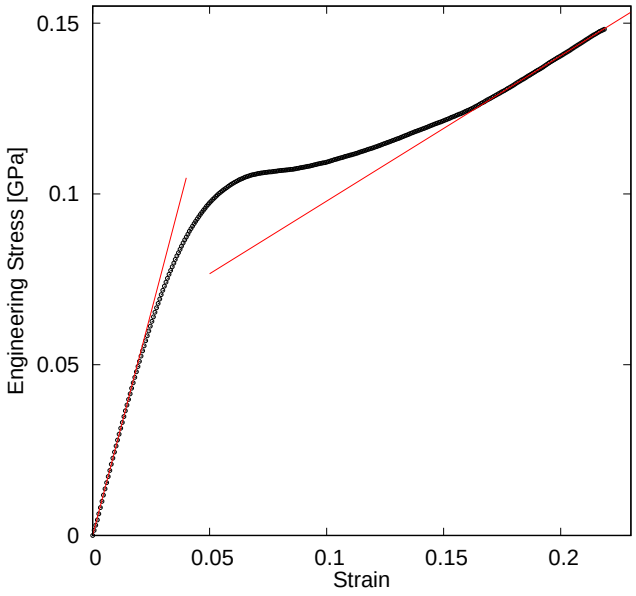

Fig. 1. Engineering stress, $\sigma = F / A$ (F is the drawing force and $A = N / \sum_1^N 1/A_i$ is the average cross sectional area of the fiber), as a function of engineering strain, $\varepsilon = (L - L_0)/L_0$ (L is the current length of the fibre and L_0 the initial length), for an un-annealed Zeonex fibre. The straining rate ($\dot{\varepsilon} = d\varepsilon / dt = (1/L_0) \cdot dL / dt$) is 1.1%/s.

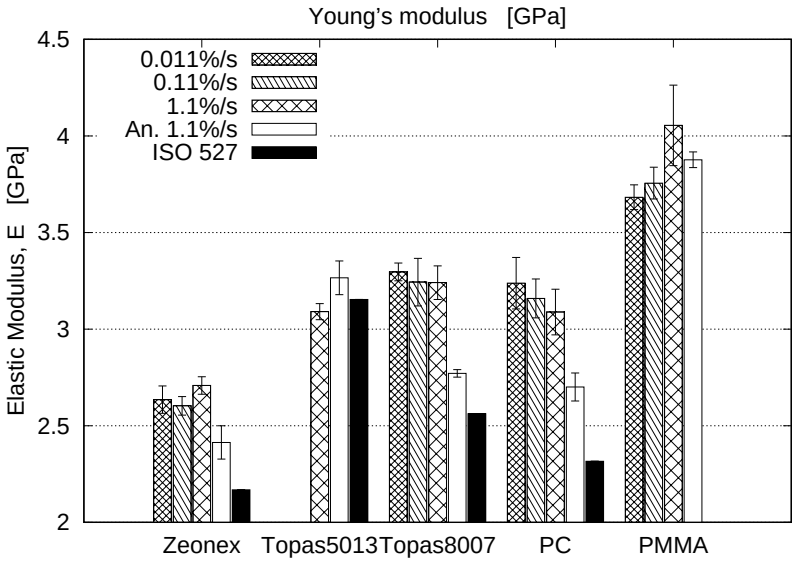

Fig. 2. Average elastic modulus E, calculated on the whole statistical group of tested fibres. The error bars represent ± one standard deviation. Figure 1. The individual elastic modulus E are calculated from the initial linear slope, $\sigma = E \cdot \varepsilon$, between the engineering stress (σ) and strain (ε) as illustrated in Fig. 1. The straining rate, $\dot{\varepsilon}$, range from 0.011%/s to 1.1%/s. The elastic modulus (multiplied with a geometrical factor of 0.9856) reported by the manufacturers based on an ISO 527 standard are shown as well.

Optical Materials EXPRESS

3.1 Elastic modulus

In sensing of small energetic deformations, such as vibration and sound, it is the elastic modulus E that is the important quantity defining fibre sensitivity [22]. Ideally, the initial linear slope of the relation between the measured stress $\sigma = F / A$ and strain ε of the sample defines the elastic modulus $\sigma = F / A$. With small fluctuations in the fibre diameter the sample is not theoretically ideal. Though, due to the very large ratio between the length and diameter, we can use a slender fibre approximation during the straining. This assumes that the sample deforms with pure extension, i.e. no shear. In this case, the local stress is $\sigma = F / A_i$. From a series of local force balances it can be shown that in the linear stress-strain region the relation $F \cdot (1/N) \sum_1^N 1/A_i = E \cdot \varepsilon$. Its derivation ideally requires a rate independent elastic modulus. As discussed later, this is not a real concern here. The average cross-sectional area A, then has to be calculated from $A = N / \sum_1^N 1/A_i$ to obtain the theoretically correct elastic modulus, as the slope of the linear relation between stress and strain. This is shown in Fig. 1, which shows an example of a stress-strain curve measured for a Zeonex fibre. The E modulus has been calculated from a least square fitting in the initial linear region of the curve which, in most cases, is up to strains of 0.01, i.e. 1%. In all the figures in this paper presenting engineering stress versus engineering strain, the engineering strain is based on the overall sample length and the average area A has been used in the calculation of the engineering stress.

The elastic modulus of the tested POFs are depicted in Fig. 2. Notice that the ordinate (E modulus) axis is initiated on a value of 2 GPa. The values are averages of a number (5-7) of measured samples. The only exception is the un-annealed Topas 5013S-04 POFs where only 4 samples were tested and only at one drawing speed. All error bars presented in all the figures here represent ± one standard deviation.

3.2 Statistical analysis

From an engineering point of view, it is important to know to what extend a specific sample will deviate from an average value. It is particularly important to know if there exists a maximal possible deviation from the mean value, implying an actual understanding of the underlying probability distribution. The causes of the scattering are likely to be unknown, and in all the figures presented here we use error bar as ± one standard deviation, i.e. a total width of two standard deviations. In the case of the elastic modulus in Fig. 2, the standard deviations are, on average, as low as 2% of the modulus value.

It is possible to evaluate graphically whether or not the mean values are statically different, based on the least square error bars. If the difference between two mean values is less than the sum of their standard deviations, graphically if the error bars overlap, they are on a (maximal) 89% confidence level not different. Further if the difference is more than the sum of two of their standard deviations (the sum of the full length of the error bars) they are on an about 99.7% confidence level different. These confidence levels are based on 6 samples measured at each set of testing conditions.

3.3 Effect of straining rate and annealing on the elastic modulus

The samples were all tested at a constant straining rate defined as $\dot{\varepsilon} = d\varepsilon / dt = (1/L_0) \cdot dL / dt$. In percent strain, the rates were 0.011%/s, 0.11%/s and 1.1%/s for the un-annealed fibres and 1.1%/s for the annealed ones. Inspecting the straining rate dependency of the elastic modulus for all the un-annealed POFs, there seems not to be any significant difference between the average values. Our results are in line with similar observations of statistically insignificant sensitivity toward extension rates in [50], where un-aligned Zeonex 690R, PC and PMMA polymer sample were measured in compression. This

Optical Materials EXPRESS

also implies that the frequency dependency of the stress sensing in the linear elastic area is not essential for the use of any of tested POFs. This is in agreement with the very low frequency sensitivity of the elastic modulus, which is on the scale of about 1-2% change per decade change in frequency, observed on un-aligned amorphous polymers [51]. A recent paper reports an increase of the elastic modulus with frequency for dynamic (DMA) [29–31] testing of POFs. Most of the samples tested in ref [29] are from the same polymers as the ones used in this work. An increase of fibre's elastic modulus on the level of 10% per decade of frequency increase was observed. This would represent a change of about ten times the standard deviations on our measurements.

The reduction of elastic modulus due to the annealing process is significant in the case of Zeonex 480R, PC Makrolon LED2245 and Topas 8007S-04 POFs. They display a significant reduction in the elastic modulus of 10-15% after the annealing. The annealing of Topas 5013S-04 and PMMA (GEHR) POFs is without any statistically significant effect on the fibre elastic modulus. We have also made a comparison with the elastic modulus reported by the manufacturers [34,35,37,36]. Notice we have multiplied these elastic moduli with a geometrical factor of 0.9856 to account for the lack of internal microstructure, which are present in the mPOFs. The microstructure accounts (ideally) for 1.44% of the cross sectional area perpendicular to the drawing direction. The elastic moduli reported by the manufacturers are expected to represent the behaviour of bulk randomly oriented polymers. Although moulding of the 'dog-boned' shaped test samples may involve some polymeric structuring, we would expect it to be considerably smaller than the molecular alignment resulting from the fibre drawing. In the case of the Topas 5013S-04, the manufacturer-reported value is the same as the one obtained here for the POFs. For the POFs reducing their elastic modulus due to annealing, there still seems to be a further potential for a reduction in their modulus with respect to the modulus of corresponding bulk materials.

The annealing may also affect the dimensions of the POFs. Table 1 shows the average fibre diameter before and after annealing. Notice that it was not measured on the same samples before and after the annealing. For both Topas POFs there is no significant change in dimension. The other POFs do increase their diameter after annealing.

Optical Materials EXPRESS

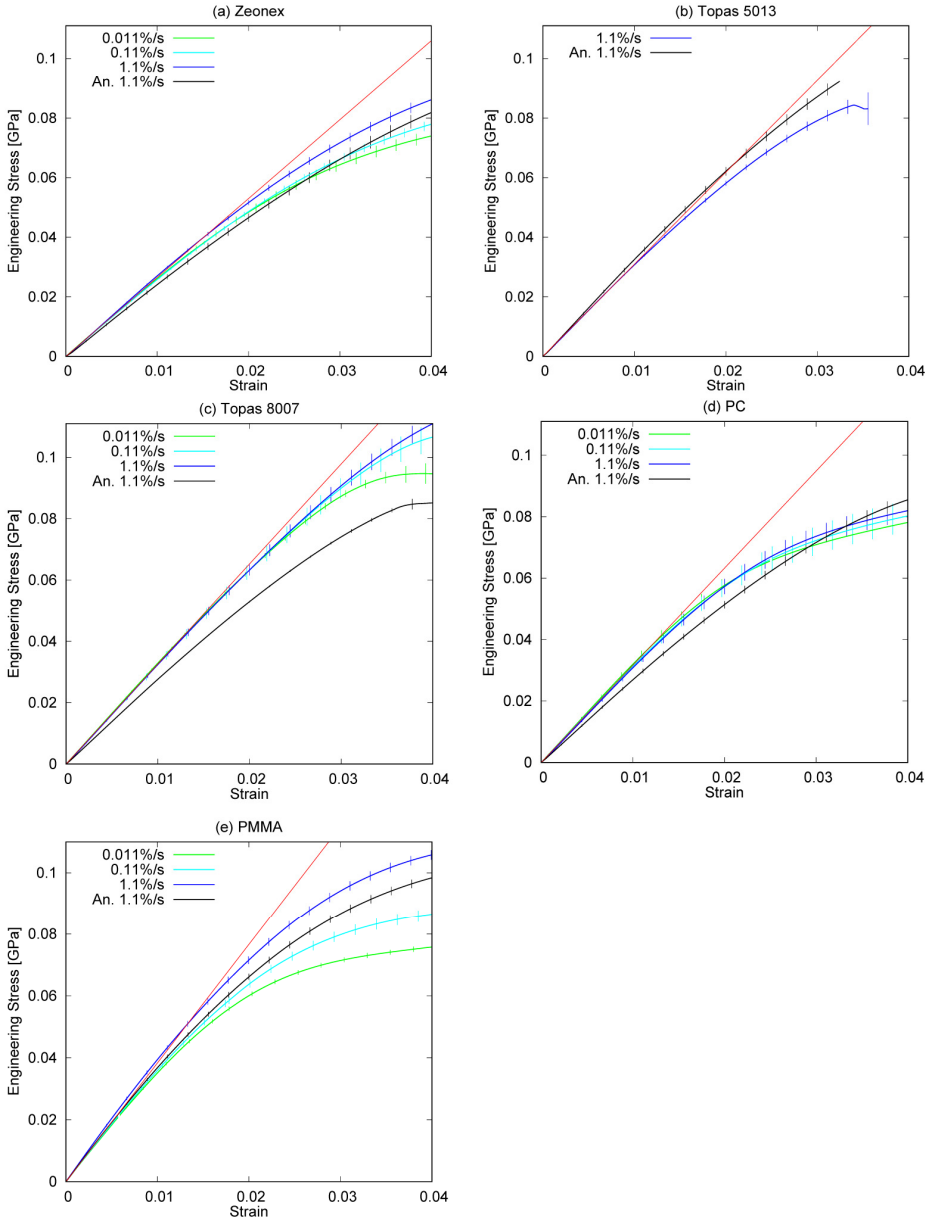

Fig. 3. Engineering stress, $\sigma = F / A$ (F is the drawing force and $A = N / \sum_1^N 1 / A_i$ is the average cross sectional area of the fiber), as a function of engineering strain, $\varepsilon = (L - L_0) / L_0$ (L is the current length of the fibre and L_0 the initial length) in the elastic region for the un-annealed and annealed POFs strained at different straining rates ($\dot{\varepsilon} = d\varepsilon / dt = (1 / L_0) \cdot dL / dt$). The un-annealed POFs were strained at rates, $\dot{\varepsilon}$, of 011%/s. (green line), 0.11%/s (light blue line) and 1.1%/s (dark blue line). The annealed POFs were strained at a rate, $\dot{\varepsilon}$, of 1.1%/s (black line). The error bars represent ± one standard deviation. The red line is the linear elasticity, based on an overall average for the un-annealed fibres. Figure 3(a): Zeonex 480R POFs. Figure 3(b): Topas 5013S-04 POFs. Figure 3(c): Topas 8007S-04 POFs. Figure 3(d): PC Makrolon LED2245 POFs. Figure 3(e): PMMA (GEHR) POFs.

Optical Materials EXPRESS

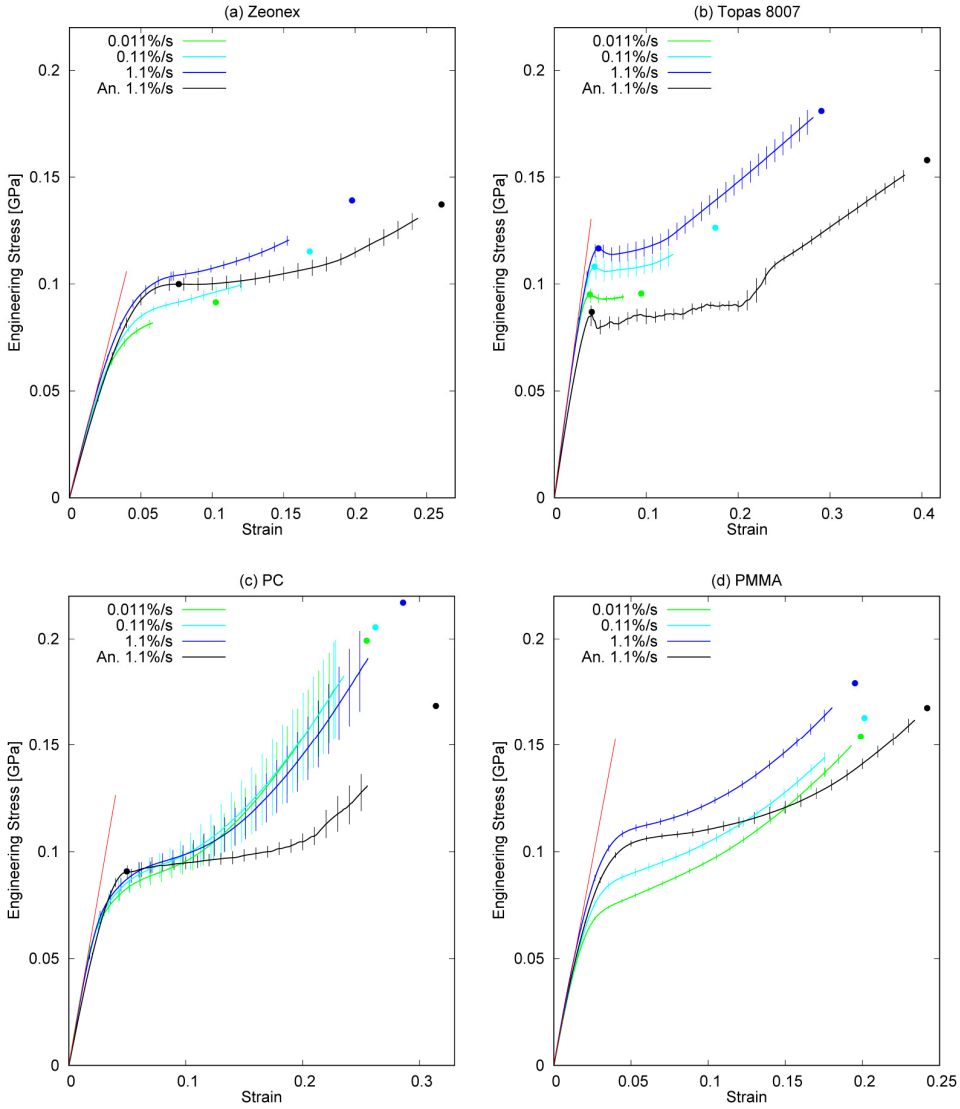

Fig. 4. Engineering stress, $\sigma = F / A$ (F is the drawing force and $A = N / \sum_1^N 1 / A_i$ is the average cross sectional area of the fiber), as a function of engineering strain, $\varepsilon = (L - L_0) / L_0$ (L is the current length of the fibre and L_0 the initial length). These are the full stress-strain curves of the un-annealed and annealed POFs strained at different straining rates. The un-annealed POFs were strained at strained at rates, $\dot{\varepsilon}$ ($\dot{\varepsilon} = d\varepsilon / dt = (1 / L_0) \cdot dL / dt$) of 0.011%/s. (green line), 0.11%/s (light blue line) and 1.1%/s (dark blue line). The annealed POFs were strained at a rate of, $\dot{\varepsilon}$, of 1.1%/s (black line). The error bars represent ± one standard deviation. The red line is the linear elasticity, E (defined in Fig. 2), based on an overall average for the un-annealed fibres. The curves are all terminated at the lowest (engineering) strain at break values observed in the experiments. The bullets represent the average yield (the first maximum on the stress-strain curve) and break points (final point on the stress-strain curve), based on the average data for the corresponding fibre type. The bullets have the same colour as the corresponding lines. The average yield points have been shown on the as the bullets on the stress strain lines. The average break of the POFs has been shown as the bullets after the stress strain lines. Figure 4(a): Zeonex 480R POFs. Figure 4(b): Topas 8007S-04. Figure 4(c): PC Makrolon LED2245 POFs. Figure 4(d): PMMA (GEHR) POFs.

Optical Materials EXPRESS

3.4 Nonlinear elasticity

In Fig. 3, stress-strain curves averaged from all tested samples of respective fibre type are shown until a strain of 4% for all involved POFs. Notice, all error bars displayed in the figures represent ± one standard deviation. In the nonlinear elasticity region, from a strain of about 1%, all the POFs show a significant and nontrivial effect of the annealing, comparing measurements at the same straining speed (1.1%/s). The referred annealed and un-annealed POFs are represented by the blue and black curves in Fig. 3, respectively. More importantly, the general insensitivity of the elastic modulus toward straining rate [50] does not hold in the nonlinear elastic region. Polycarbonate Makrolon LED2245 POF is the only one, which is statically insensitive to the straining rate, though it has a relative large data scattering compared to the other POFs. These observations are in agreement with the compression measurements presented in ref [50] for un-aligned Zeonex 690R and a Polycarbonate. Topas 8007S-04 POF shows no sensitivity to the straining rate until a strain of 3%, whereas the PMMA POF is the one most sensitive to the change in the straining rate. Notice that the Topas 5013S-04 POF breaks before it reaches the yield stress.

3.5 Yield

By definition, the yield stress and strain is determined as the location of the (first) maximum on the stress strain curve. It is classically considered as the limit of reversibility in the material elasticity, although, in most cases it is the onset of instability associated with a local nonhomogeneous deformation, i.e. necking, in the sample. The reversibility in strained polymeric samples is of more complex nature [50,52–54]. In Fig. 4, complete stress-strain curves averaged over all tested samples of respective fibre type are shown until sample break for all involved POFs. The average yield point has been added to the graphs as a dot on the stress-strain curves as well. The curves are all terminated at the lowest strain at break observed in the measurement of the respective POF type at given conditions. Topas 8007S-04 POF is the only fibre showing a yield point in all cases. The effects of the nonhomogeneous deformation are particular apparent for the annealed Topas 8007S-04 POFs. All the stress strain curves for Topas 8007S-04, including the mean curves showed in Fig. 4(b), exhibit a high level of irregularity due to the inhomogeneous deformation. This effect appears until the stress increases above the yield stress value. In technical use, the yield and following sample inhomogeneity is an unwanted effect if the fibre should be used at high strain values. The annealing lowers the stress levels experienced by the fibre at the same straining rate for all tested POFs. Most importantly, the lower slope of the stress-strain curves after annealing makes the fibres more sensitive to inhomogeneous deformations. The Zeonex 480R and PC Makrolon LED2245 POFs show a yield point only in the annealed case, but the weak straining rate dependency of the stress-strain curve will have a stabilizing effect on a localized necking phenomenon in the case of the Zeonex 480R POFs. Actually, the clear lack of a yield point in the un-annealed POFs will stabilize the fibre deformation and allow the fibres to be uses at very high strain values.

Optical Materials EXPRESS

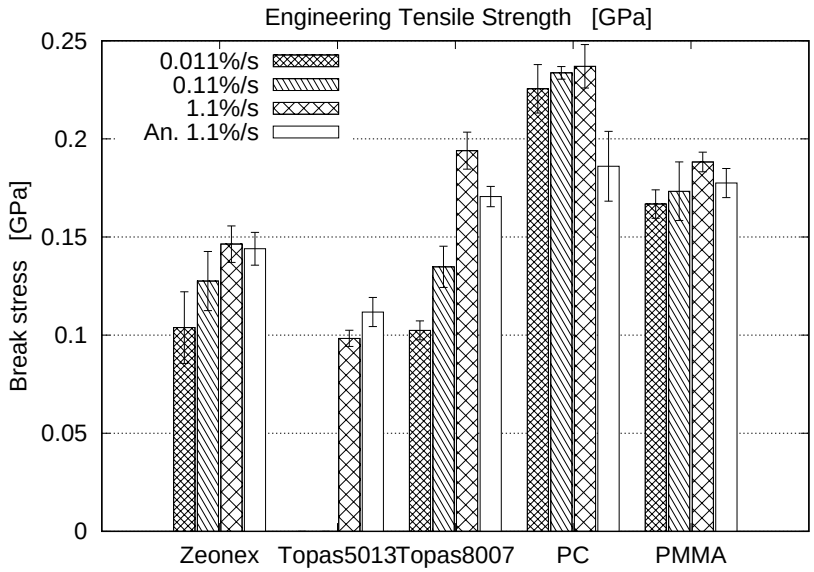

Fig. 5. Engineering stress at break for all investigated POFs tested at various conditions. The engineering stress of break is calculated as $\sigma = F / \min(A_i)$ where $\min(A_i)$ is the smallest cross-sectional area on the fiber and F is the drawing force. The error bars represent ± one standard deviation. The un-annealed POFs are strained at rates, $\dot{\varepsilon}$, of 0.011%/s, 0.11%/s and 1.1%/s while the annealed POFs are strained at 1.1%/s.

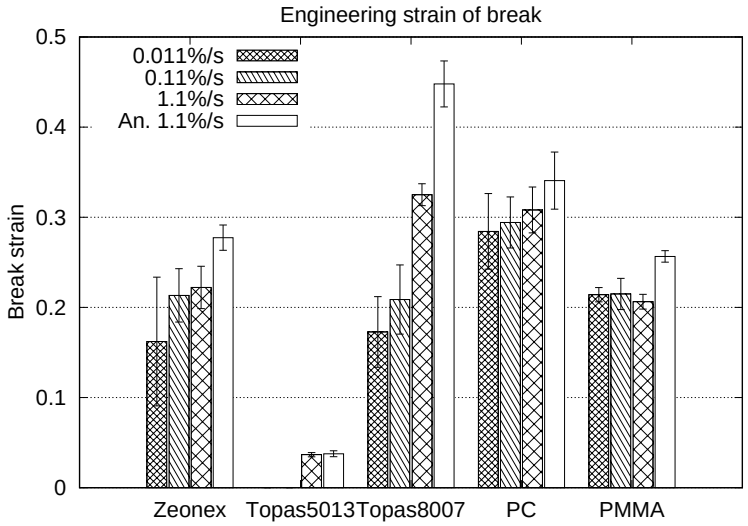

Fig. 6. Corrected Engineering strain at break for all investigated POFs tested at various conditions. The corrected Engineering strain at break are calculated as $\varepsilon_b = \varepsilon_c A / \min(A_i) + \varepsilon_0 \left(1 - A / \min(A_i)\right)$. The terminal linear behaviour of the stress-strain curve (illustrated in Fig. 1) has an intersection with the strain axis at ε_0 and strain at break is ε_c. $A = N / \sum_1^N 1/A_i$ is the average cross sectional area of the fiber and $\min(A_i)$ the smallest cross-sectional area on the fiber. The error bars represent ± one standard deviation. The un-annealed POFs are strained at rates, $\dot{\varepsilon}$, of 0.011%/s, 0.11%/s and 1.1%/s while the annealed POFs are strained at 1.1%/s.

Optical Materials EXPRESS

3.6 Break

Like the 'necking' phenomenon, the fracture of the POFs is an unwanted effect. The 'necking' is predictable from the time dependent stress-strain relation, whereas the fracture depends on the plasticity of the polymers interacting with microscopic imperfections inside or on the surface of the POFs. A prediction of the break would require knowledge of the initial (surface) imperfections and the underlying plastic behaviour of the polymers, which is of much more complex nature that the measured stress-strain relations presented here.

In Fig. 4 the curves are all terminated at the lowest strain at break value observed in the experiments, where the average break point of the POF has been shown as the dot after the stress strain curve. These engineering stress and strain values in Fig. 4 are based on the average cross-sectional area and total length of the sample. The correct engineering stress and strain is a local value. The fibre break and the yield will appear at the thinnest position of the sample. Therefore, the correct engineering stress of break and yield stress is calculated at this position as $\sigma = F / \min(A_i)$. These engineering stress at break values are shown in Fig. 5. The correct strain is at this thinnest position as well. It can be calculated with the use of the slender fibre approximation, similar to the correction of the elastic modulus, where the terminal linear behaviour of the stress-stain curve is used here. An example of the data analysis of the terminal linear behaviour on one measurement has been shown in Fig. 1, where the engineering stress and strain values are based on the average area and total length of the sample. The terminal linear behaviour of the stress-strain curve (see Fig. 1) has an intersection with the strain axis at ε_0 and an average-based strain at break of ε_c. From these values, the correct strain at break can be calculated as $\varepsilon_b = \varepsilon_c \frac{A}{\min(A_i)} + \varepsilon_0 \left(1 - \frac{A}{\min(A_i)}\right)$.

In Fig. 6, these corrected engineering strain at break values are shown. Its derivation has been based on local force balances and the assumption of time independency. This correction formula should only be used in the case of small fluctuation in the fibre diameters, as the time dependency in the stress-strain curves may have an effect on the corrected strain. This is not a real issue in the case of the PC (Makrolon LED2245) and PMMA (GEHR) as they show statistically insignificant straining rate, or time, dependency with regard to their stress and strain at break. This is in contrast to the performance of Topas 8007S-04, which shows sensitivity to the straining rate, as seen in Fig. 5 and 6. Notice, the PMMA (GEHR) does show a clear rate dependency of the overall stress levels but not of the critical break stress and strain.

The alignment of the polymers seems to have large consequences on the fracturing of the POFs. Topas 5013S-04 were reported to have a critical strain as low as 0.017 under the standard testing conditions [35], whereas POFs drawn from this material exhibits critical strain above 0.03 as seen in Fig. 3(b). For PC Makrolon LED2245, the critical strain at standard testing conditions was reported as high as 1.2 [37], while the strain at break of the PC POFs was less than 0.4. The annealing did not reduce the strain at break in any of the POFs. All observed effects may not be a consequence of the alignment alone. The shaping of the surface of the drawn POFs may contribute to the sensitivity on the onset of crack development as well. During the drawing of cane into fibre, surface imperfections would be expected to originate from impurities. These are difficult to quantify compared to surface irregularities from machined or moulded polymers.

The data scattering of the break stress and strain data is on the scale of about ± 4% (PMMA GEHR) to ± 50% (Zeonex 480R). It is of particular interest to notice the severe increase in the (relative) data scattering of the Zeonex (480R) and Topas 8007S-04 at low straining rates in Fig. 6. From engineering point of view, the important quantity is the lowest possible strain at break. For Zeonex (480R) values as low as about 0.1 have been observed, while the critical strain at break for bulk samples at standard testing condition is 0.4 [36]. The

Optical Materials EXPRESS

breaking mechanism and crack development in these POFs, presumably due to the alignment of polymer chains, is very sensitive to variation of straining rate.

4. Summary and conclusions

Five different polymers have been drawn into POFs; two copolymers: Topas 5013S-04 and 8007S-04; and three different homopolymers: Zeonex (480R), PC (Makrolon LED2245) and PMMA (GEHR). These polymers have all previously been drawn into microstructured POFs and used in fibre sensing applications. With a drawing Hencky strain of about 12 the polymeric configurations and consequently internal stresses are homogeneously distributed in the fibres. Furthermore, with drawing stresses from 1 to 10 times the value of the extensional plateau modulus (3G_N^0) of the polymers, the polymer molecules are highly aligned in the drawing direction in the POFs after drawing. This alignment of the polymers has large impact on the fibre mechanical behaviour.

Within the linear elastic limit, until a strain of about 1%, we have observed no significant straining rate dependence for all tested POFs within two decade change of the straining rate, for the un-annealed fibres. Temperature annealing of the POFs (Topas 8007S-04, Zeonex and PC) reduces the fibre elastic modulus by 10-15% towards the standard elastic modulus of the bulk material. Drawn POF from Topas 5013S-04 already exhibited modulus value close to the standard modulus of the bulk material.

In the nonlinear elastic region, only the PC POF is statistically unaffected by the changes in straining rate, though showing larger data scattering than the other POFs. A clear unconditional yield is only present in the Topas 8007S-04 POF. The polymer alignment actively stabilizes the remaining POFs against nonhomogeneous deformations, i.e. ‘neckings’. The annealing flattens stress-strain curves for all tested POFs, thus making them more sensitive to necking. Notice that the Topas 5013S-04 POFs break before they yield. The Topas 5013S-04 was reported to have a strain at break as low as 1.7% for the un-aligned bulk material at standard testing conditions, whereas the POFs break at a strain above 3%.

The fracturing of the POFs is very sensitive to the alignment of the polymers. All strains at break values of PC Makrolon LED2245 are statically independent of straining rate, though the annealing affects the stress-strain curve. All the PC Makrolon LED2245 POFs break at strains below 40% while the bulk PC at standard testing conditions breaks at a strain of 120%. Contrary to the PC as well as the PMMA (GEHR) POFs, the strain at break for the Zeonex 480R and Topas 8007S-04 POFs is highly straining rate dependent. At low straining rate, the strain at break of the Zeonex 480R POFs is as low as 10% compared to 40% of the standard bulk material case.

The study reveals the crucial differences between mechanical behaviour of nominally similar POFs prepared from various materials and provides new valuable information for selection of suitable POF material with regard to applications where fibre mechanical performance is of importance, e.g. strain and stress sensing.

Funding

People Programme (Marie Curie Actions) of the European Union's Seventh Framework Programme FP7/2007-2013/ under REA grant agreement n° 608382.

References

1. M. C. J. Large, G. W. Barton, L. Poladian, and M. A. van Eijkelenborg, Microstructured Polymer Optical Fibres (Springer, 2008).
2. D. J. Webb, “Polymer Fiber Bragg Grating Sensors and Their Application,” in Optical Fiber Sensors: Advanced Techniques and Applications, G. Rajan, ed. (CRC Press, 2015).
3. K. Peters, “Polymer optical fiber sensors — a review,” Smart Mater. Struct. **20**(1), 013002 (2011).
4. J. Jensen, P. Hoiby, G. Emiliyanov, O. Bang, L. Pedersen, and A. Bjarklev, “Selective detection of antibodies in microstructured polymer optical fibers,” Opt. Express **13**(15), 5883–5889 (2005).
5. G. Emiliyanov, J. B. Jensen, O. Bang, P. E. Hoiby, L. H. Pedersen, E. M. Kjaer, and L. Lindvold, “Localized biosensing with Topas microstructured polymer optical fiber,” Opt. Lett. **32**(5), 460–462 (2007).

Optical Materials EXPRESS

6. U. Hassan, J. Janting, S. Aasmul, and O. Bang, "Polymer Optical Fiber Compound Parabolic Concentrator fiber tip based glucose sensor: in-Vitro Testing," IEEE Sens. J. **16**(23), 8483–8488 (2016).
7. G. Emiliyanov, P. E. Høiby, L. H. Pedersen, and O. Bang, "Selective serial multi-antibody biosensing with TOPAS microstructured polymer optical fibers," Sensors (Basel) **13**(3), 3242–3251 (2013).
8. D. Shan, C. Zhang, S. Kalaba, N. Mehta, G. B. Kim, Z. Liu, and J. Yang, "Flexible biodegradable citrate-based polymeric step-index optical fiber," Biomaterials **143**, 142–148 (2017).
9. M. van Eijkelenborg, M. Large, A. Argyros, J. Zagari, S. Manos, N. Issa, I. Bassett, S. Fleming, R. McPhedran, C. M. de Sterke, and N. A. Nicorovici, "Microstructured polymer optical fibre," Opt. Express **9**(7), 319–327 (2001).
10. M. C. J. Large, G. W. Barton, L. Poladian, and M. A. van Eijkelenborg, Microstructured Polymer Optical Fibres (Springer, 2008).
11. A. Argyros, "Microstructures in Polymer Fibres for Optical Fibres, THz Waveguide, and Fibre-Based Metamaterials," ISRN Optics, 785162 (2013).
12. G. D. Peng, Z. Xiong, and P. L. Chu, "Photosensitivity and gratings in dye-doped polymer optical fibers," Opt. Fiber Technol. **5**(2), 242–251 (1999).
13. Z. Xiong, G. D. Peng, B. Wu, and P. L. Chu, "Highly tunable Bragg gratings in single-mode polymer optical fibers," IEEE Photonics Technol. Lett. **11**(3), 352–354 (1999).
14. T. Wang, Q. Wang, Y. Luo, W. Qiu, G.-D. Peng, B. Zhu, Z. Hu, G. Zou, and Q. Zhang, "Enhancing photosensitivity in near UV/vis band by doping 9-vinylanthracene in polymer optical fiber," Opt. Commun. **307**, 5–8 (2013).
15. W. Zhang, A. Abang, D. J. Webb, and G.-D. Peng, "Wavelength Drift of PMMA-Based Optical Fiber Bragg Grating Induced by Optical Absorption," IEEE Photonics Technol. Lett. **27**(4), 336–339 (2015).
16. C. Markos, A. Stefani, K. Nielsen, H. K. Rasmussen, W. Yuan, and O. Bang, "High-Tg TOPAS microstructured polymer optical fiber for fiber Bragg grating strain sensing at 110 degrees," Opt. Express **21**(4), 4758–4765 (2013).
17. K. Nielsen, H. K. Rasmussen, A. J. L. Adam, P. C. M. Planken, O. Bang, and P. U. Jepsen, "Bendable, low-loss Topas fibers for the terahertz frequency range," Opt. Express **17**(10), 8592–8601 (2009).
18. A. Fasano, G. Woyessa, P. Stajanca, C. Markos, A. Stefani, K. Nielsen, H. K. Rasmussen, K. Krebber, and O. Bang, "Fabrication and characterization of polycarbonate microstructured polymer optical fibers for hightemperature-resistant fiber Bragg grating strain sensors," Opt. Mater. Express **6**(2), 649 (2016).
19. G. Woyessa, A. Fasano, C. Markos, A. Stefani, H. K. Rasmussen, and O. Bang, "Zeonex microstructured polymer optical fiber: fabrication friendly fibers for high temperature and humidity insensitive Bragg grating sensing," Opt. Mater. Express **7**(1), 286 (2017).
20. A. Lacraz, M. Polis, A. Theodosiou, C. Koutsides, and K. Kalli, "Femtosecond Laser Inscribed Bragg Gratings in Low Loss CYTOP Polymer Optical Fiber," IEEE Photonic. Tech. Lett. **27**(7), 693–696 (2015).
21. M. Koerdt, S. Kibben, J. Hesselbach, C. Brauner, A. S. Herrmann, F. Vollertsen, and L. Kroll, "Fabrication and characterization of Bragg gratings in a graded-index perfluorinated polymer optical fiber," Procedia Technology **15**, 138–146 (2014).
22. A. Stefani, S. Andresen, W. Yuan, N. Herholdt-Rasmussen, and O. Bang, "High sensitivity polymer optical fiber-bragg-grating-based accelerometer," IEEE Photonics Technol. Lett. **24**(9), 763–765 (2012).
23. A. Stefani, W. Yuan, S. Andresen, and O. Bang, "Dynamic characterization of polymer optical fibers," IEEE Sens. J. **12**(10), 3047–3053 (2012).
24. I.-L. Bundalo, K. Nielsen, G. Woyessa, and O. Bang, "Long-term strain response of polymer optical fiber FBG sensors," Opt. Mater. Express **7**(3), 967–976 (2017).
25. W. Yuan, L. Khan, D. J. Webb, K. Kalli, H. K. Rasmussen, A. Stefani, and O. Bang, "Humidity insensitive TOPAS polymer fiber Bragg grating sensor," Opt. Express **19**(20), 19731–19739 (2011).
26. D. Bosc and C. Toinen, "Tensile mechanical properties and reduced internal stresses of polymer optical fiber," Polym. Compos. **14**(5), 410–413 (1993).
27. C. H. Jiang, M. G. Kuzyk, J. L. Ding, W. E. Johns, and D. J. Welker, "Fabrication and mechanical behavior of dye-doped polymer optical fiber," J. Appl. Phys. **92**(1), 4–12 (2002).
28. P. Stajanca, O. Cetinkaya, M. Schukar, P. Mergo, D. J. Webb, and K. Krebber, "Molecular alignment relaxation in polymer optical fibers for sensing applications," Opt. Fiber Technol. **28**, 11–17 (2016).
29. A. Leal-Junior, A. Frizera, M. J. Pontes, A. Fasano, G. Woyessa, O. Bang, and C. A. F. Marques, "Dynamic mechanical characterization with respect to temperature, humidity, frequency and strain in mPOFs made of different materials," Opt. Mater. Express **8**(4), 804–815 (2018).
30. Mechanical properties characterization of polymethyl methacrylate polymer optical fibers after thermal and chemical treatments.
31. Dynamic Mechanical Analysis on a PolyMethyl Methacrylate (PMMA) Polymer Optical Fiber.
32. GEHR GmbH, "Technical Data Sheet – GEHR PMMA®," http://www.gehrplastics.com/products-and-applications/material/acrylic.html.
33. I. P. Johnson, W. Yuan, A. Stefani, K. Nielsen, H. K. Rasmussen, L. Khan, D. J. Webb, K. Kalli, and O. Bang, "Optical fibre Bragg grating recorded in TOPAS cyclic olefin copolymer," Electron. Lett. **47**(4), 271–272 (2011).
34. TOPAS Advanced Polymers Inc, "Technical data sheet - TOPAS® 8007S-04," (TOPAS Advanced Polymers Inc., 2017), https://Topas.com/sites/default/files/TDS_8007S-04_e_EU.pdf.

Optical Materials EXPRESS

35. TOPAS Advanced Polymers Inc, "Technical data sheet - TOPAS® 5013S-04," (TOPAS Advanced Polymers Inc., 2017), https://Topas.com/sites/default/files/ TDS_5013S–04_e_EU.pdf.
36. ZEON corporation, "ZEON Cyclo Olefin Polymer (COP) ZEONEX," (ZEON corporation 2016), http://www.zeon.co.jp/content/200181690.pdf.
37. Covestro, "Makrolon LED2245," (Covestro 2017), file:///C:/Users/hkra/Downloads/Makrolon_LED2245_ISO_en%20(1).pdf.
38. S. C. Xue, R. I. Tanner, G. W. Barton, R. Lwin, M. C. J. Large, and L. Poladian, "Fabrication of Microstructure Optical Fibres. Part I: Problem Formulation and Numerical Modelling of Transient Draw Process," J. Lightwave Technol. **23**(7), 2245–2254 (2005).
39. S. C. Xue, R. I. Tanner, G. W. Barton, R. Lwin, M. C. J. Large, and L. Poladian, "Fabrication of Microstructured Optical Fibres. Part II: Numerical Modeling of Steady-State Draw Process," J. Lightwave Technol. **23**(7), 2255–2266 (2005).
40. L. J. Fetters, D. J. Lohse, D. Richter, T. A. Witten, and A. Zirkel, "Connection between Polymer Molecular Weight, Density, Chain Dimensions, and Melt Viscoelastic Properties," Macromolecules **27**(17), 4639–4647 (1994).
41. A. Bach, K. Almdal, H. K. Rasmussen, and O. Hassager, "Elongational Viscosity of Narrow Molar Mass Distribution Polystyrene," Macromolecules **36**(14), 5174–5179 (2003).
42. K. Kalli and D. J. Webb, "Polymer Optical Fiber-Based Sensors," in Advanced Fiber Optics: Concepts and Technology, L. Thévenaz, ed. (EPFL Press, 2011).
43. H. K. Rasmussen and Q. Huang, "Interchain tube pressure effect in extensional flows of oligomer diluted nearly monodisperse polystyrene melts," Rheol. Acta **53**(3), 199–208 (2014).
44. A. Bach, H. K. Rasmussen, and O. Hassager, "Extensional viscosity for polymer melts measured in the filament stretching rheometer," J. Rheol. (N.Y.N.Y.) **47**(2), 429–441 (2003).
45. N. Zhong, M. Zhao, Q. Liao, X. Zhu, Y. Li, and Z. Xiong, "Effect of heat treatments on the performance of polymer optical fiber sensor," Opt. Express **24**(12), 13394–13409 (2016).
46. C. A. F. Marques, A. Pospori, G. Demirci, O. Çetinkaya, B. Gawdzik, P. Antunes, O. Bang, P. Mergo, P. André, and D. J. Webb, "Fast bragg grating inscription in PMMA polymer optical fibres: impact of thermal pre-treatment of preforms," Sensors (Basel) **17**(4), 891 (2017).
47. A. Pospori, C. A. F. Marques, D. Sáez-Rodríguez, K. Nielsen, O. Bang, and D. J. Webb, "Thermal and chemical treatment of polymer optical fiber Bragg grating sensors for enhanced mechanical sensitivity," Opt. Fiber Technol. **36**, 68–74 (2017).
48. A. Fasano, G. Woyessa, J. Janting, H. K. Rasmussen, and O. Bang, "Solution-Mediated Annealing of Polymer Optical Fiber Bragg Gratings at Room Temperature," IEEE Photonics Technol. Lett. **29**(8), 687–690 (2017).
49. A. Stefani, K. Nielsen, H. K. Rasmussen, and O. Bang, "Cleaving of TOPAS and PMMA microstructured polymer optical fibers: core-shift and statistical quality optimization," Opt. Commun. **285**(7), 1825–1833 (2012).
50. V. Srivastava, S. A. Chester, N. M. Ames, and L. Anand, "A thermo-mechanically-coupled large-deformation theory for amorphous polymers in a temperature range which spans their glass transition," Int. J. Plast. **26**(8), 1138–1182 (2010).
51. N. Lagakos, J. Jarzynski, J. H. Cole, and J. A. Bucaro, "Frequency and temperature dependence of elastic moduli of polymers," J. Appl. Phys. **59**(12), 4017–4031 (1986).
52. B. Crist, "Yield processes in glassy polymers," in The Physics of Glassy Polymers, R. N. Haward and R. J. Young, ed. (Springer Science & Business Media, 1997).
53. J. Rottler and M. O. Robbins, "Yield conditions for deformation of amorphous polymer glasses," Phys. Rev. E Stat. Nonlin. Soft Matter Phys. **64**(5), 051801 (2001).
54. C. Chui and M. C. Boyce, "Monte Carlo Modeling of Amorphous Polymer Deformation: Evolution of Stress with Strain," Macromolecules **32**(11), 3795–3808 (1999).